IOP Publishing Journal of Physics B: Atomic, Molecular and Optical Physics
J. Phys. B: At. Mol. Opt. Phys. **49** (2016) 125304 (16pp) doi:10.1088/0953-4075/49/12/125304

Mean-field regime and Thomas–Fermi approximations of trapped Bose–Einstein condensates with higher-order interactions in one and two dimensions

Xinran Ruan[1], **Yongyong Cai**[2,3] **and Weizhu Bao**[1]

[1] Department of Mathematics, National University of Singapore, Singapore 119076
[2] Beijing Computational Science Research Center, No. 10 West Dongbeiwang Road, Haidian District, Beijing 100193, People's Republic of China
[3] Department of Mathematics, Purdue University, West Lafayette, IN 47907, USA

E-mail: yongyong.cai@gmail.com and matbaowz@nus.edu.sg

Received 5 November 2015, revised 16 March 2016
Accepted for publication 20 April 2016
Published 20 May 2016

Abstract

We derive rigorously one- and two-dimensional mean-field equations for cigar- and pancake-shaped Bose–Einstein condensates (BECs) with higher-order interactions (HOIs), which originate from shape-dependent confinement corrections to the effective two-body atomic interaction potential. We show how the higher-order interaction modifies the contact interaction of the strongly confined particles. Surprisingly, we find that the usual Gaussian profile assumption for the strongly confining direction is inappropriate for the cigar-shaped BEC case, and a Thomas–Fermi-type profile should be adopted instead. Based on the derived mean-field equations, the Thomas–Fermi densities are analyzed in the presence of the contact interaction and HOI, and considering the limit of large contact interaction and HOI. For both box and harmonic traps in one, two and three dimensions, we identify the analytical Thomas–Fermi densities, which depend on the competition between the contact interaction and the HOI.

Keywords: Bose–Einstein condensate, dimension reduction, higher-order interaction, Thomas–Fermi approximation, modified Gross–Pitaevskii equation

(Some figures may appear in colour only in the online journal)

1. Introduction

Quantum-degenerate gases have been explored extensively ever since the remarkable discovery of Bose–Einstein condensate (BEC) in 1995 [1–3]. In typical BEC experiments, the ultra-cold bosonic gases are dilute and interact weakly, where only two-body interactions are relevant. As a result, the major properties of the system are governed by these weak two-body interactions [4–6]. Ideally, the BEC system is described by the Hamiltonian for N identical bosons with binary interactions as

$$H_N = \sum_{k=1}^{N}\left(-\frac{\hbar^2}{2m}\nabla_{\mathbf{x}_k}^2 + V(\mathbf{x}_k)\right) + \sum_{1\leqslant j<k\leqslant N} V_{\rm int}(\mathbf{x}_j - \mathbf{x}_k),$$

where $V(\mathbf{x})$ is an external trapping potential, $V_{\rm int}$ is the interatomic potential, $\mathbf{x}_k$ is the spatial coordinates for the kth atom, $\hbar$ is the reduced Planck constant, m is the mass of the particle and N is the total number of particles. The Gross–Pitaevskii equation (GPE) for BEC, a mean-field approximation for the above N-body Hamiltonian [6, 7], contains two key assumptions. Firstly, the GP theory assumes that the N-body wave function $\Psi(\mathbf{x}_1, \ldots, \mathbf{x}_N, t)$ is the product of the single wave functions $\psi(\mathbf{x}_k, t)$, i.e. the mean-field approximation,

$$\Psi(\mathbf{x}_1, \ldots, \mathbf{x}_N, t) \approx \prod_{k=1}^{N} \psi(\mathbf{x}_k, t). \tag{1}$$

Secondly, although the atomic interaction potentials are rather complicated, they can be described effectively by the two-

body Fermi contact interaction—the interaction kernel taken as the Dirac delta function $\delta(\cdot)$—in the ultra-cold dilute regime, with a single parameter, the zero energy s-wave scattering length a_s, i.e.

$$V_{\rm int}(\mathbf{x}_j - \mathbf{x}_k) = V_{\rm mf}(\mathbf{x}_j - \mathbf{x}_k) := g_0\delta(\mathbf{x}_j - \mathbf{x}_k), \tag{2}$$

and $g_0 = \frac{4\pi\hbar^2 a_s}{m}$. The above two assumptions lead to the well-known cubic nonlinear Schrödinger equation, which is also known as the GPE, where the nonlinearity arises from the effective interaction potential approximation. This effective δ potential is the heart of the mean-field GPE theory for BEC [6, 7]. Based on the GPE, various aspects of BEC have been extensively studied, including the static properties [7–9] and dynamic properties [10–12].

The treatment of effective two-body contact interactions has been proven to be successful, but it is limited due to the low energy or low density assumption [13]. In the case of high particle densities or strong confinement, there will be a wider range of possible momentum states and correction terms should be included in the GPE to provide a better results [14, 15]. In [15, 16], shape-dependent confinement corrections to the effective potential have been explained and derived as

$$V_{\rm int}(\mathbf{x}_j - \mathbf{x}_k) = V_{\rm mf}(\mathbf{x}_j - \mathbf{x}_k) + V_{\rm hoi}(\mathbf{x}_j - \mathbf{x}_k), \tag{3}$$

where

$$V_{\rm hoi}(\mathbf{x}) = \frac{g_0 g_1}{2}[\delta(\mathbf{x})\nabla^2 + \nabla^2\delta(\mathbf{x})], \tag{4}$$

and $g_1 = \frac{a_s^2}{3} - \frac{a_s r_e}{2}$ with r_e being the effective range of the two-body interactions. Within the perturbation framework, taking the above higher-order interaction (HOI) (or effective range expansion) $V_{\rm hoi}$ into account, a modified GPE (MGPE), which is equation (5), is obtained by inserting (3) into the N-body Hamiltonian with the mean-field approximation [15–18].

Based on the MGPE (5), [19–21] have shown the stability conditions and collective excitations of a harmonically trapped BEC. In the Thomas–Fermi (TF) limit regime (large particle number), [22] showed the approximate density profile for BEC with HOI in a radial trap. On the other hand, in most experiments, a strong harmonic trap is applied along one or two directions to confine (or suppress) the condensate into a pancake or cigar shape, respectively. In such cases, the usual TF approximation for the full three-dimensional (3D) case becomes invalid. It is then desirable to derive the effective one- (1D) and two-dimensional (2D) models, which offer compelling advantages for numerical computations compared to the 3D case.

In this paper, we present effective mean-field equations for trapped BECs with HOI in one and two dimensions. Our equations are based on a mathematically rigorous dimension reduction of the 3D MGPE (5) to lower dimensions. Such dimension reduction has been formally derived in [9, 23–27] and rigorously analyzed in [28, 29], for the conventional GPE, i.e. without HOI. While for the MGPE, to our knowledge, this result has not been obtained, except for some preliminary works [17, 21], where the Gaussian profile is assumed in the strongly confining direction following the conventional GPE case. Surprisingly, our findings suggest that the Gaussian profile assumption is inappropriate for the quasi-1D BEC. In the derivation of the quasi-1D (2D) model for the BEC with HOI, we assume that the leading order (in terms of aspect ratio) of the full 3D energy is from the radial (longitudinal) wave function, such that the BEC can only be excited in the non-confining directions, resulting in effective 1D (2D) condensates. Based on this principle, we show that the longitudinal wave function can be taken as the ground state of the longitudinal harmonic trap in quasi-2D BEC, and the radial wave function has to be taken as the TF type (see (11)) in quasi-1D BEC, which is totally different from the conventional GPE case [17, 21]. Furthermore, we derive simple TF densities in 1D, 2D and 3D from our effective equations, with different HOI and contact interaction parameters, for both harmonic and box potentials. These results yield very interesting phase diagrams of the TF ground-state densities regarding the contact interaction and HOI. We compare the ground states of the quasi-1D and quasi-2D BEC with the ground states of the full 3D BEC and find good agreement. In particular, our ground states are good approximations to those of the full 3D MGPE in regimes where the TF approximation fails.

The paper is organized as follows. In section 2, we introduce the modified GPE in the presence of HOI that will be considered in this paper. As the first main result, we present in section 3 the mean-field equation for the quasi-1D cigar-shaped BEC. We compare the ground-state solutions of this 1D equation with the full 3D computation. In section 4, we present the second main result, the mean-field equation for the quasi-2D pancake-shaped BEC. Comparisons are made between ground-state density profiles of the 2D equation and ground-state density profiles calculated from the full 3D model. In section 5, we provide a complete summary of the TF approximations in 1D, 2D and 3D cases, with harmonic potential or box potential separately. Depending on the HOI strength and contact interaction strength, the TF approximations are surprisingly different in different regimes, which are shown in figure 3, and they are compared with the corresponding ground-state solutions obtained via mean-field equations. Finally, we present our conclusions in section 6. Appendix A provides the details of the dimension reduction from the full 3D MGPE to our 1D mean-field equation, and appendix B provides the details for the reduction to the 2D case.

2. 3D modified GPE

At temperature T much lower than the critical temperature T_c, the mean-field GPE of a BEC may include the HOI effect [15, 21]. Inserting the HOI correction into the two-body interaction potential, we can obtain the MGPE [16, 17] for the

wave function $\psi := \psi(\mathbf{x}, t)$ as

$$\mathrm{i}\hbar\partial_t\psi = \left[-\frac{\hbar^2}{2m}\nabla^2 + V + g_0(|\psi|^2 + g_1\nabla^2|\psi|^2)\right]\psi, \quad (5)$$

where $\mathbf{x} = (x, y, z)^T \in \mathbb{R}^3$ is the Cartesian coordinate vector, $g_0 = \frac{4\pi\hbar^2 a_s}{m}$ is the contact interaction strength.

The last unusual nonlinear term (not present for conventional GPE [6, 7]) accounts for the HOI correction to the effective two-body interaction potential [15, 16], which is nonlocal and the strength is given by the parameter $g_1 = \frac{a_s^2}{3} - \frac{a_s r_e}{2}$. For the hard sphere potential case, $r_e = \frac{2}{3}a_s$. $V := V(\mathbf{x})$ is the given real-valued external trapping potential. As in typical current experiments, we assume that the BEC is confined in the following harmonic potential

$$V(\mathbf{x}) = \frac{m}{2}[\omega_x^2 x^2 + \omega_y^2 y^2 + \omega_z^2 z^2], \quad (6)$$

where $\omega_x > 0$, $\omega_y > 0$ and $\omega_z > 0$ are trapping frequencies in x-, y- and z-direction, respectively. The wave function ψ is normalized as

$$\|\psi(\cdot, t)\|^2 := \int_{\mathbb{R}^3} |\psi(\mathbf{x}, t)|^2 \mathrm{d}\mathbf{x} = N, \quad (7)$$

where N is the total number of particles in BEC.

We introduce the dimensionless quantities by rescaling length, time, energy and wave function as $\mathbf{x} \to \mathbf{x}x_s$, $t \to t/\omega_0$, $E \to E\hbar\omega_0$ and $\psi \to \psi\sqrt{N/x_s^3}$, respectively, where $x_s = \sqrt{\frac{\hbar}{m\omega_0}}$ with $\omega_0 = \min\{\omega_x, \omega_y, \omega_z\}$. After rescaling, the dimensionless form of the MGPE (5) reads

$$\mathrm{i}\partial_t\psi = -\frac{1}{2}\nabla^2\psi + V(\mathbf{x})\psi + \beta|\psi|^2\psi - \delta\nabla^2(|\psi|^2)\psi, \quad (8)$$

with

$$\beta = 4\pi N\frac{a_s}{x_s}, \quad \delta = -\frac{4\pi N}{x_s^3}\left(\frac{a_s^3}{3} - \frac{a_s^2 r_e}{2}\right), \quad (9)$$

and the dimensionless trapping potential is $V(\mathbf{x}) = \gamma_x^2 x^2/2 + \gamma_y^2 y^2/2 + \gamma_z^2 z^2/2$ with $\gamma_x = \omega_x/\omega_0$, $\gamma_y = \omega_y/\omega_0$ and $\gamma_z = \omega_z/\omega_0$. The normalization condition becomes

$$\|\psi(\cdot, t)\|^2 = \int_{\mathbb{R}^3} |\psi(\mathbf{x}, t)|^2 \mathrm{d}\mathbf{x} = 1. \quad (10)$$

When $\delta = 0$, the MGPE (8) collapses to the conventional GPE and the corresponding dimension reduction problem has been studied in [9, 23–28] and references therein. When $\delta < 0$, there is no ground state of (8), and when $\delta > 0$ and the trapping potential is a confinement, there are ground states of (8) and the positive ground state is unique if $\beta \geqslant 0$. Thus hereafter we assume $\delta > 0$.

3. Quasi-1D BEC with HOI

With a sufficiently large radial trapping frequency, it is possible to freeze the radial motion of a BEC [30], and then we have a quasi-1D system. Intuitively, the energy separation between stationary states is much larger in the radial direction than in the axial direction, and the dynamics is then frozen in radial direction. As a consequence, the wave function of the system is in the variable separated form, i.e., it is the multiplication of the axial direction function and the radial direction function. In this section, we present an effective mean-field equation for the axial wave function of the BEC with HOI, by assuming a strong radial confinement.

3.1. 1D mean-field equation

In order to derive the mean-field equation for the axial wave function, we start with the 3D MGPE (5) and assume a harmonic potential with $\omega_r = \omega_x = \omega_y \gg \omega_z$. Choosing the rescaling parameters used in (8) as $\omega_0 = \omega_z$, $x_s = \sqrt{\hbar/m\omega_z}$, we now work with the dimensionless equation (8). In the quasi-1D BEC with HOI, the 3D wave fuction can be factorized as

$$\psi(\mathbf{x}, t) = \mathrm{e}^{-\mathrm{i}\mu_{2D}t}\chi_{2D}(x, y)\psi_{1D}(z, t), \quad (11)$$

with appropriate radial state function χ_{2D} and $\mu_{2D} \in \mathbb{R}$. Once the radial state χ_{2D} is known, we could project the MGPE (8) onto the axial direction to derive the quasi-1D equation. The key to find such χ_{2D} is the criterion that the energy separation between stationary states should be much larger in the radial direction than in the axial direction, i.e., there is an energy scale separation between the radial state χ_{2D} and the axial wave function.

We denote the aspect ratio of the harmonic trap as

$$\gamma = \omega_r/\omega_z. \quad (12)$$

For the conventional GPE, i.e., $\delta = 0$, a good choice for χ_{2D} is the Gaussian function [9], which is the ground state of the radial harmonic trap, as $\chi_{2D}(r) = \sqrt{\frac{\gamma}{\pi}}\mathrm{e}^{-\frac{\gamma r^2}{2}}$. The reason is that the order of the energy separation between states of the conventional BEC is dominated in the radial direction by the radial harmonic oscillator part, which is $O(\gamma)$, much larger than the interaction energy part if $\beta = O(1)$ by a similar computation shown in appendix A. Alternatively, it would be possible to use a variational Gaussian profile approach to find $\chi_{2D}(r)$ [25]. In a similar dimension reduction problem for cold Fermi gases [32], the profile χ_{2D} is chosen based on comparison between energy levels of the harmonic oscillator and Fermi energy. For a BEC with HOI, the extra HOI term contributes to the energy. Thus, a more careful comparison between the kinetic energy part and the HOI energy part is needed.

By detailed computation (see appendix A), we identify the energy contribution from the HOI term (A5) in transverse direction to be dominant when $\gamma \gg 1$. This is a completely different scenario as compared to the conventional GPE, in which the transverse harmonic oscillator terms are dominant. The explicit form for the transverse radial state function $\chi_{2D}(r)$ for the quasi-1D BEC with HOI is determined as

$$\chi_{2D}(x, y) \approx \frac{\gamma(R^2 - r^2)_+}{4\sqrt{2\delta_r}}, \quad r = \sqrt{x^2 + y^2}, \quad (13)$$

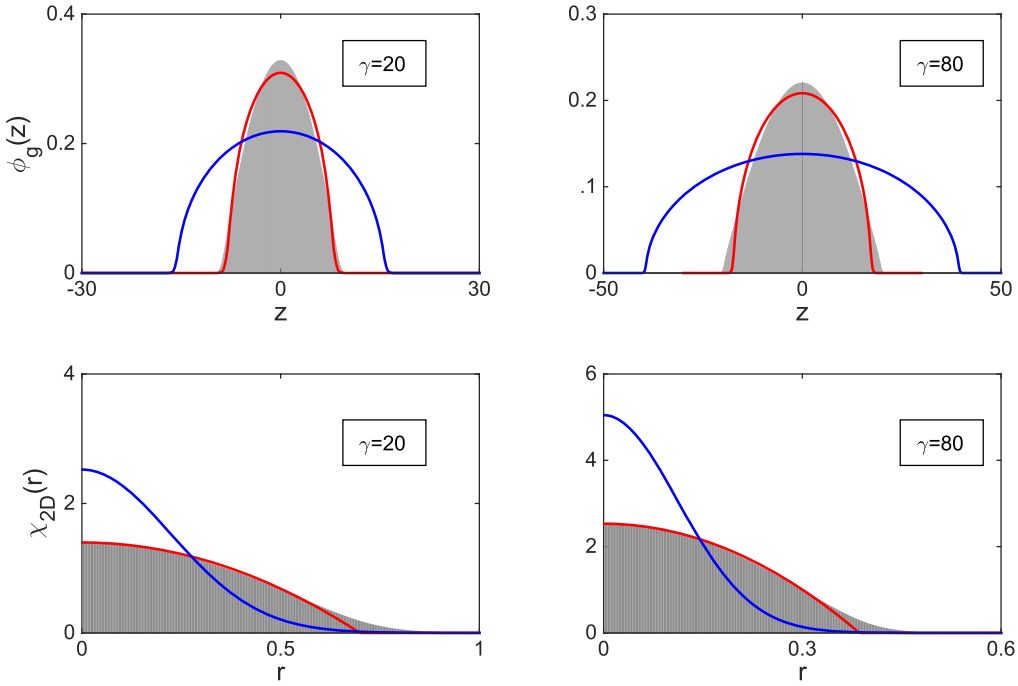

Figure 1. Quasi-1D ground state. Red line: approximation (13) in radical direction and numerical solution of (14) in axial direction. Blue line: traditional Gauss approximation in radical direction and corresponding numerical solution in axial direction. Shaded area: numerical solution from the original 3D model (8). The corresponding γs are given in the plots. For other parameters, we choose $\beta = 1$, $\delta = 20$.

where $R = 2\left(\frac{3\delta_r}{2\pi\gamma^2}\right)^{\frac{1}{6}}$, $\delta_r = \frac{2\cdot 3^{\frac{5}{7}}\pi^{\frac{1}{7}}\delta^{\frac{6}{7}}}{5^{\frac{9}{7}}\gamma^{\frac{4}{7}}}$, $\mu_{2D} \approx \frac{3^{\frac{4}{7}}\delta^{\frac{2}{7}}\gamma^{\frac{8}{7}}}{\pi^{\frac{2}{7}}5^{\frac{3}{7}}}$ and $(f)_+ = \max\{f, 0\}$.

It is worth pointing out that the determination of the radial state $\chi_{2D}(r)$ is coupled with the axial direction state (see (A3)). Therefore, a coupled system of the radial and axial states is necessary to get more refined approximate density profiles for ground states, as compared to the above approximation $\chi_{2D}(r)$.

In the axial z-direction, multiplying (8) by χ_{2D} and integrating the x, y variables, we obtain the mean-field equation for the quasi-1D BEC with HOI as

$$\begin{aligned} \mathrm{i}\partial_t\psi_{1D}(z,t) &= -\frac{1}{2}\partial_{zz}\psi_{1D} + V_{1D}(z)\psi_{1D} \\ &\quad +\beta_1|\psi_{1D}|^2\psi_{1D} - \delta_1(\partial_{zz}|\psi_{1D}|^2)\psi_{1D}, \end{aligned} \tag{14}$$

where $V_{1D}(z) = \frac{1}{2}\gamma_z^2 z^2 = \frac{1}{2}z^2$, and

$$\beta_1 = \frac{5^{\frac{6}{7}}}{3^{\frac{1}{7}}\cdot 4\pi^{\frac{3}{7}}}\delta^{\frac{3}{7}}\gamma^{\frac{12}{7}} + \frac{3^{\frac{10}{7}}}{4\cdot 5^{\frac{4}{7}}\pi^{\frac{5}{7}}}\frac{\beta\gamma^{\frac{6}{7}}}{\delta^{\frac{2}{7}}}, \tag{15a}$$

$$\delta_1 = \frac{3^{\frac{10}{7}}}{4\cdot 5^{\frac{4}{7}}\pi^{\frac{5}{7}}}\delta^{\frac{5}{7}}\gamma^{\frac{6}{7}}. \tag{15b}$$

From equation (14), it is observed that the HOI provides extra repulsive contact interactions in the quasi-1D BEC. More interestingly, the first term in β_1 suggests that the contact interaction is dominated by the HOI part.

If the repulsive contact interaction dominates the dynamics in (14), we could neglect the kinetic and HOI parts to obtain an analytical expression for the quasi-1D BEC with HOI. This agrees with the usual TF approximation for a conventional quasi-1D BEC, and its validity is shown in section 5 (referred to as region I). In such situation, the approximate density profile is given as:

$$n_{1D}(z) = |\psi_{1D}|^2 = \frac{((z^*)^2 - z^2)_+}{2\beta_1}, \tag{16}$$

where $z^* = \left(\frac{3\beta_1}{2}\right)^{\frac{1}{3}}$.

In figure 1, we compare the ground-state densities of quasi-1D BEC with HOI determined via (14) and the numerical results from 3D MGPE in (8) by integrating over the transversal directions. As shown in the figure, our proposed 1D equation, equations (13), and (14) describe the BEC accurately in axial and radical directions separately, while the traditional Gaussian approximation totally fails.

4. Quasi-2D BEC with HOI

In this section, we consider the BEC being strongly confined in the axial direction, which corresponds to the case $0 < \gamma \ll 1$. Accordingly, we choose rescaling parameters used in (8) as $\omega_0 = \omega_r$, $x_s = \sqrt{\hbar/m\omega_r}$, and we work with the dimensionless equation (8).

Similar to the case of quasi-1D BEC, we assume that the wave function can be factorized in the quasi-2D case as

$$\psi(\mathbf{x}, t) = \mathrm{e}^{-\mathrm{i}\mu_{1D}t}\psi_{2D}(x, y, t)\chi_{1D}(z), \tag{17}$$

for appropriate longitudinal state $\chi_{1D}(z)$ and $\mu_{1D} \in \mathbb{R}$.

Following the same procedure as that for the quasi-1D BEC case, we find that the leading-order energy separation in the z-direction is due to the longitudinal harmonic oscillator, while the cubic interaction and HOI parts are less important

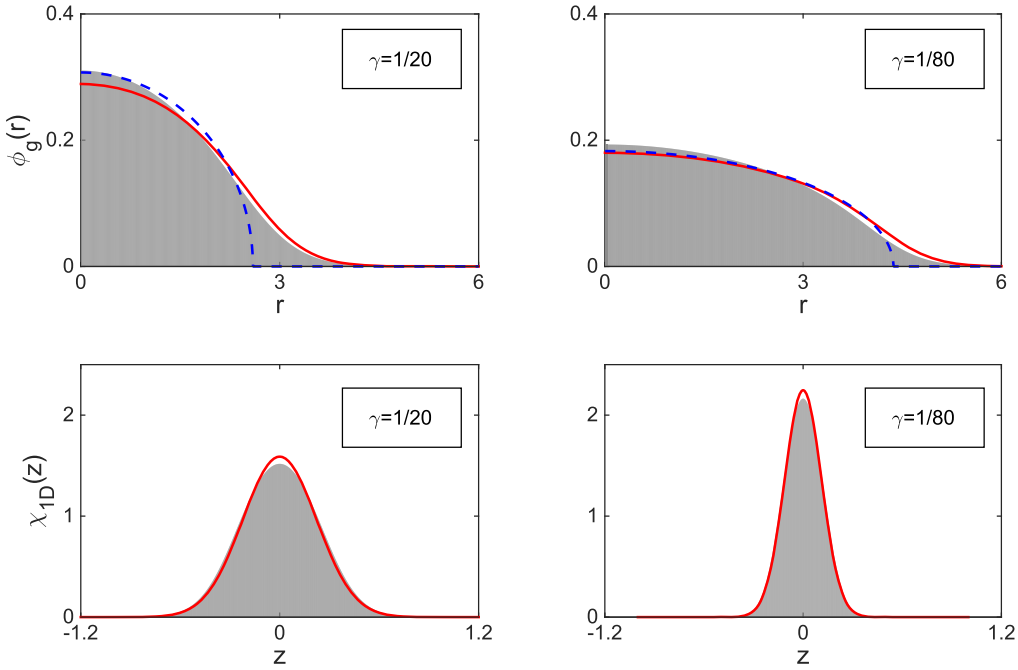

Figure 2. Quasi-2D ground state. Red line: approximation (18) in axial direction and numerical solution of (19) in radical direction. Blue dashed line: Thomas-Fermi approximation of (21) in radical direction. Shaded area: numerical solution from the original 3D model (8). The corresponding γ's are given in the plots. For other parameters, we choose $\beta = 5$, $\delta = 1$.

(see appendix B for details). This fact suggests that the ground mode of the longitudinal harmonic oscillator, i.e. a Gaussian type function, is a suitable choice for $\chi_{1D}(z)$. To be more specific,

$$\chi_{1D}(z) \approx \left(\frac{1}{\pi\gamma}\right)^{\frac{1}{4}} \mathrm{e}^{-\frac{z^2}{2\gamma}}, \tag{18}$$

and $\mu_{1D} \approx 1/2\gamma$.

Substituting (17) with (18) into the MGPE (8), then multiplying (8) by χ_{1D} and integrating the longitudinal z out, we obtain the mean-field equation for the quasi-2D BEC with HOI as

$$\begin{aligned} \mathrm{i}\partial_t \psi_{2D} = &-\frac{1}{2}\nabla^2\psi_{2D} + V_{2D}(x, y)\psi_{2D} \\ &+ \beta_2 |\psi_{2D}|^2\psi_{2D} - \delta_2(\nabla^2 |\psi_{2D}|^2)\psi_{2D}, \end{aligned} \tag{19}$$

where $V_{2D}(x, y) = \frac{1}{2}(x^2 + y^2)$ and

$$\beta_2 = \frac{\beta}{\sqrt{2\pi\gamma}} + \frac{\delta}{\sqrt{2\pi\gamma^3}}, \quad \delta_2 = \frac{\delta}{\sqrt{2\pi\gamma}}. \tag{20}$$

Similar to the quasi-1D BEC case, HOI induces effective contact interaction in the quasi-2D regime, which dominates the contact interaction (β part). We then conclude that even for small HOI δ, the contribution of HOI could be significant in the high particle density regime of quasi-2D BEC.

Analogous to the quasi-1D BEC case, we can derive the usual TF approximation when the repulsive interaction β_2 dominates the dynamics, and the analytical density for the quasi-2D BEC with HOI reads as

$$n_{2D}(r) = |\psi_{2D}|^2 = \frac{(R^2 - r^2)_+}{2\beta_2}, \quad r = \sqrt{x^2 + y^2}, \tag{21}$$

where $R = \left(\frac{4\beta_2}{\pi}\right)^{\frac{1}{4}}$.

In order to verify our findings in this section, we compare the quasi-2D ground-state densities obtained via equation (19), TF density (21) and the numerical results from the 3D MGPE (8) by integrating z out. The results are displayed in figure 2. The BEC is broadened compared to the analytically predicated profile because of the effective repulsive interaction from the HOI. Thus, in the regime of small or moderate interaction energy β_2, the usual approach to BECs with HOI via conventional TF approximation fails. On the other hand, it turns out that our proposed 2D equation, equation (19), is accurate for quasi-2D BEC in the mean-field regime at experimentally relevant trap aspect ratios γ.

5. TF approximation

In previous sections, we have derived 1D (14) and 2D (19) equations for the quasi-1D and quasi-2D BECs, respectively. Indeed, all the 1D (14), 2D (19) and 3D (8) equations can be written in a unified form as

$$\mathrm{i}\partial_t\psi = -\frac{1}{2}\nabla^2\psi + V(\mathbf{x})\psi + \beta|\psi|^2\psi - \delta\nabla^2(|\psi|^2)\psi, \tag{22}$$

where $\mathbf{x} \in \mathbb{R}^d$, $d = 3, 2, 1$, β and $\delta > 0$ are parameters. Though $V(\mathbf{x})$ is assumed to be harmonic potential in the previous derivation, it is not necessary to restrict ourselves for the harmonic potential case. Thus, we treat $V(\mathbf{x})$ as a general real-valued potential in this section. In particular, we will address the cases when $V(\mathbf{x})$ is a radially symmetric harmonic

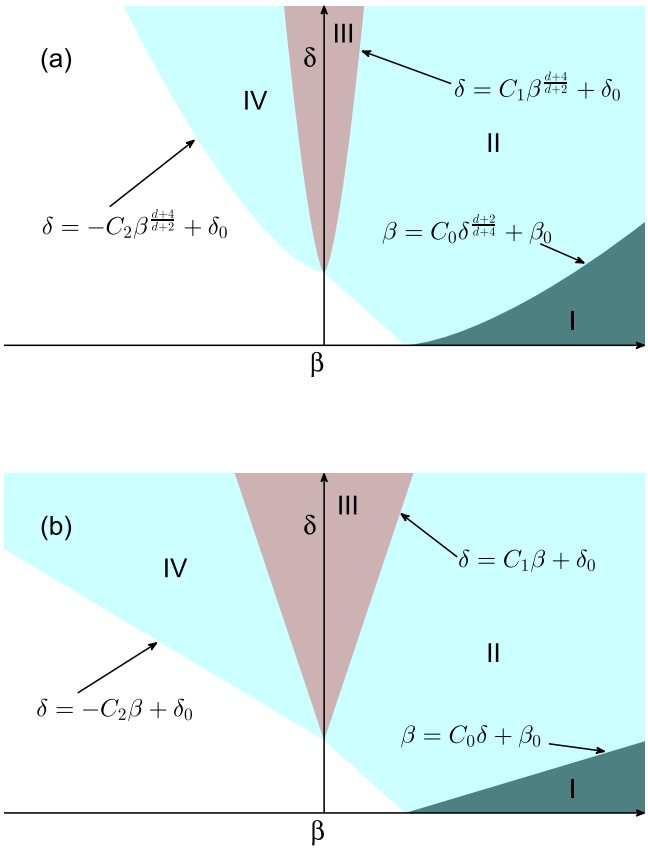

Figure 3. Phase diagram for extreme regimes: (a) is for harmonic potential case and (b) is for box potential case. In the figure, we choose $\beta_0 \gg 1$ and $\delta_0 \gg 1$, and C_0, C_1 and C_2 positive constants.

potential as

$$V(\mathbf{x}) = \frac{1}{2}\gamma_0^2 r^2, \qquad r = |\mathbf{x}|, \tag{23}$$

where $\gamma_0 > 0$ is a dimensionless constant, or a radial box potential as

$$V_{\text{box}}(\mathbf{x}) = \begin{cases} 0, & 0 \leqslant r < R, \\ \infty, & r \geqslant R. \end{cases} \tag{24}$$

As pointed out in the quasi-1D, 2D cases, analogous to the conventional BEC, a dominant repulsive contact interaction will lead to analytical TF densities. However, with HOI (22), the system is characterized by two interactions, contact interaction strength β and HOI strength δ, which is totally different from the classical GPE theory where the BEC is purely characterized by the contact interaction β. Hence, for BEC with HOI (22), it is possible that HOI competes with contact interaction, and may be the major effect determining the properties of BEC. In this section, we will discuss how the competition between β and δ leads to different density profiles for the strong interactions ($|\beta|$, $\delta \gg 1$), where the kinetic energy term is always dropped (see discussion below), and we refer to such analytical density approximations as TF approximations [7]. We notice that it might not be necessary to consider HOI as the key factor of BEC in three dimensions in current BEC experiments, but we treat δ and β in (22) as arbitrary parameters and the result presented here may find applications in future and/or in other fields.

In previous sections on quasi-1D and 2D BECs, we have given the analytical TF densities for a β dominant system. For the general consideration of the large β and δ interactions, we show in figure 3 the phase diagram of the different parameter regimes for β and δ, in which the TF approximation are totally different. Intuitively, there are three of them: the β term is more important (regime I in figure 3), the δ term is more important (regime III), and the β term is comparable to the δ term (regimes II and IV). Detailed computations and arguments for the regimes shown in figure 3 can be found in appendix C. Based on figure 3, we will discuss the harmonic potential case and the box potential case separately.

5.1. TF approximation with harmonic potential

From figure 3(a), the curve $\beta = O(\delta^{\frac{d+2}{d+4}})$ is the boundary that divides the regimes for harmonic potential case. To be more specific, if $\beta \gg \delta^{\frac{d+2}{d+4}}$, the cubic nonlinear term is more important, and vise versa. If $\beta = O(\delta^{\frac{d+2}{d+4}})$, both of the two nonlinear terms are important, and have to be taken care of in the TF approximation. The resulting analytical TF density profiles in different regimes, are listed below:

Regime I: i.e. $\beta \gg \delta^{\frac{d+2}{d+4}}$, the δ term and the kinetic energy term are dropped, and the density profile is determined as

$$n_{\text{TF}}(r) = |\psi_{\text{TF}}|^2 = \frac{\gamma_0^2(R^2 - r^2)_+}{2\beta}, \tag{25}$$

where $R = \left(\frac{(d+2)\tilde{C}_d\beta}{\gamma_0^2}\right)^{\frac{1}{d+2}}$, and the constant $\tilde{C}_d$ is defined as

$$\tilde{C}_d = \begin{cases} \frac{1}{2}, & d = 1, \\ \frac{1}{\pi}, & d = 2, \\ \frac{3}{4\pi}, & d = 3. \end{cases} \tag{26}$$

With the above TF densities, the leading-order approximations for chemical potential μ and energy E of the ground state are: $\mu_{\text{TF}} = \frac{1}{2}((d+2)\tilde{C}_d\beta)^{\frac{2}{d+2}}\gamma_0^{\frac{2d}{d+2}}$, $E_{\text{TF}} = \frac{d+2}{d+4}\mu_{\text{TF}}$ for the d ($d = 3, 2, 1$) dimensional case.

Regime II: i.e. $\beta = C_0\delta^{\frac{d+2}{d+4}}$ with $C_0 > 0$, neglecting the kinetic term in the time-independent MGPE, we have

$$\mu\psi = \frac{\gamma_0^2|\mathbf{x}|^2}{2}\psi + C_0\delta^{\frac{d+2}{d+4}}|\psi|^2\psi - \delta\nabla^2(|\psi|^2)\psi. \tag{27}$$

Formally, equation (27) degenerates at position $\mathbf{x}$ if $\psi(\mathbf{x}) = 0$ and it is indeed a free boundary problem (boundary of the zero level set of ψ), which requires careful consideration. Motivated by [22] for the 3D case, we impose $n'(R) = 0$ besides the condition that $n(R) = 0$ along the free boundary $|\mathbf{x}| = R$, and we assume $n(r) = 0$ for $r > R$.

The TF density profile in regime II is self similar under appropriate scalings. To be more specific, the analytical TF density takes the form

$$n_{\text{TF}}(r) = |\psi_{\text{TF}}|^2 = \delta^{-\frac{d}{d+4}}n_0(\delta^{-\frac{1}{d+4}}r), \tag{28}$$

where $n_0(r)$ is a function that can be calculated exactly as below.

Plugging (27) into (28), we obtain the equation for $n_0(r)$ by imposing the aforementioned conditions at the free boundary,

$$\tilde{\mu} = \frac{\gamma_0^2 r^2}{2} + C_0 n_0 - \partial_{rr} n_0(r) - \frac{d-1}{r}\partial_r n_0(r), \quad (29)$$

for $r \leqslant R$ and $n_0(s) = 0$ for $s \geqslant R$, and $n_0(R) = 0$, $n_0'(R) = 0$, where R is the free boundary that has to be determined and $\tilde{\mu} = \delta^{-\frac{2}{d+4}}\mu$. In addition, we assign the boundary condition at $r = 0$ as $n_0'(0) = 0$, because of the symmetry.

Note that C_0 can be negative as the δ term can bound the negative cubic interaction, which corresponds to regime IV. In fact, for regime IV, we will repeat the above procedure.

Denote $a = \sqrt{C_0}$ and the ordinary differential equation (29) in d dimensions can be solved analytically. Denote

$$f_{a,d}(r) = \begin{cases} \mathrm{e}^{ar} + \mathrm{e}^{-ar}, & \text{for } d = 1, \\ I_0(ar), & \text{for } d = 2, \\ (\mathrm{e}^{ar} - \mathrm{e}^{-ar})/r, & \text{for } d = 3, \end{cases} \quad (30)$$

where $I_0(r)$ is the standard modified Bessel function I_α with $\alpha = 0$. Then the solution of equation (29) with prescribed Neumann boundary conditions reads as

$$n_0(r) = -\frac{\gamma_0^2 r^2}{2a^2} + \left(\frac{\tilde{\mu}}{a^2} - \frac{d\gamma_0^2}{a^4}\right) + \frac{\gamma_0^2 R}{a^2 f_{a,d}'(R)} f_{a,d}(r). \quad (31)$$

Inserting the above expression to the normalization condition that $\int_{\mathbb{R}^d} n_0(\mathbf{x})\mathrm{d}\mathbf{x} = 1$, we find chemical potential,

$$\tilde{\mu} = \frac{\tilde{C}_d a^2}{R^d} + \frac{d\gamma_0^2 R^2}{2(d+2)}. \quad (32)$$

Combining (31) and (32), and noticing the Dirichlet condition $n(R) = 0$, we have the equation for R,

$$\left(\frac{(aR)^2}{d+2} - \frac{\tilde{C}_d a^4}{\gamma_0^2 R^d} + d\right) f_{a,d}'(R) = a^2 R f_{a,d}(R). \quad (33)$$

Thus, the free boundary R can be calculated and $n_0(r)$ is then determined.

Regime III: i.e. $\beta \ll \delta^{\frac{d+2}{d+4}}$, the β term and the kinetic energy term are dropped, and the TF density profile is

$$n_{\mathrm{TF}}(r) = |\psi_{\mathrm{TF}}|^2 = \frac{\gamma_0^2 (R^2 - r^2)_+^2}{8(d+2)\delta}, \quad (34)$$

where $R = \left(\frac{(d+2)^2(d+4)\tilde{C}_d\delta}{\gamma_0^2}\right)^{\frac{1}{d+4}}$. Again, the leading-order approximations for chemical potential and energy, with the above TF densities, are $\mu_{\mathrm{TF}} = \frac{d}{2(d+2)}((d+2)^2(d+4)\tilde{C}_d\delta\gamma_0^{d+2})^{\frac{2}{d+4}}$, $E_{\mathrm{TF}} = \frac{d+4}{d+6}\mu_{\mathrm{TF}}$ in d dimensions.

Regime IV: i.e. $\beta = -C_0\delta^{\frac{d+2}{d+4}}$ with $C_0 > 0$. By using a similar procedure as for regime II, we can get (28) and

$$\tilde{\mu} = \frac{\gamma_0^2 r^2}{2} - C_0 n_0 - \partial_{rr} n_0(r) - \frac{d-1}{r}\partial_r n_0(r), \quad (35)$$

for $r \leqslant R$ and $n_0(s) = 0$ for $s \geqslant R$, and $n_0'(0) = 0$, $n_0(R) = 0$, $n_0'(R) = 0$, where R is the free boundary that has to be determined and $\tilde{\mu} = \delta^{-\frac{2}{d+4}}\mu$. Again, let $a = \sqrt{C_0}$ and denote

$$g_{a,d}(r) = \begin{cases} \cos(ar), & \text{for } d = 1, \\ J_0(ar), & \text{for } d = 2, \\ \sin(ar)/r, & \text{for } d = 3, \end{cases} \quad (36)$$

where $J_0(r)$ is the Bessel function of the first kind $J_\alpha(r)$ with $\alpha = 0$. The solution of equation (35) with the assigned Neumann boundary conditions can be written as:

$$n_0(r) = \frac{\gamma_0^2 r^2}{2a^2} - \left(\frac{\tilde{\mu}}{a^2} + \frac{d\gamma_0^2}{a^4}\right) - \frac{\gamma_0^2 R}{a^2 g_{a,d}'(R)} g_{a,d}(r). \quad (37)$$

The chemical potential is then calculated from normalization condition as

$$\tilde{\mu} = -\frac{\tilde{C}_d a^2}{R^d} + \frac{d\gamma_0^2 R^2}{2(d+2)}. \quad (38)$$

Finally, the free boundary R is determined from the Dirichlet condition $n_0(R) = 0$,

$$\left(\frac{a^2 R^2}{d+2} + \frac{\tilde{C}_d a^4}{\gamma_0^2 R^d} - d\right) g_{a,d}'(R) = a^2 R g_{a,d}(R). \quad (39)$$

After R is computed, we then find $n_0(r)$.

In figure 4, we compare the analytical TF densities (25), (28) and (34) with the numerical results computed via the full equation (22) by the backward Euler finite difference (BEFD) method [31]. We observe that in all the extreme regions, the analytical TF densities agree very well with the full equation simulations. As a byproduct, we compare the corresponding chemical potentials and energies in figure 5.

It has been shown that the usual TF densities provide accurate approximations for the density profiles for quasi-1D an 2D BECs. Indeed, we can check that for fixed 3D parameters β and δ, the effective contact interaction β_1 and HOI δ_1 (or β_2 and δ_2) for quasi-1D (2D) condensate are in the TF regime I in the quasi-1D (2D) limit, i.e. $\gamma \to \infty$ ($\gamma \to 0^+$). This justifies that the effective contact interactions are dominant for the dynamics in the quasi-1D (2D) limit.

For instance, we know $\beta_1 \sim O(\gamma^{\frac{12}{7}})$ and $\delta_1 \sim O(\gamma^{\frac{6}{7}})$ in quasi-1D limit, and it implies that $\beta_1 \gg \delta_1^{3/5}$ as $\gamma \gg 1$. This immediately suggests that the TF density (25) is a good approximation for the density profiles in the quasi-1D limit regime, which has been shown in figure 1. In the quasi-2D limit, i.e. $\gamma \to 0^+$, we find $\beta_2 \gg \delta_2^{2/3}$ in view of $\beta_2 \sim O(\gamma^{-3/2})$ and $\delta_2 \sim O(\gamma^{-1/2})$, which again confirms that the TF density (25) is a good approximation for the density profile, as observed in figure 2.

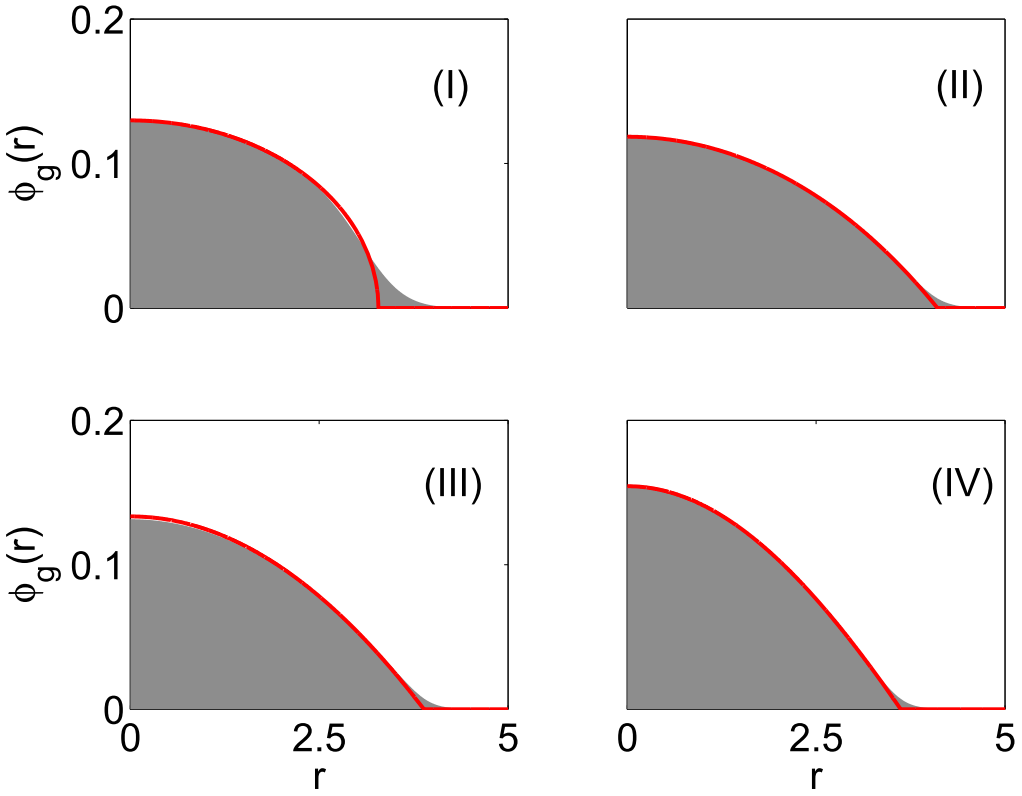

Figure 4. Comparisons of 3D numerical ground states with TF densities, the harmonic potential case in regions I, II, III and IV, which are defined in figure 3(a). Red line: Thomas–Fermi approximation, and shaded area: numerical solution from the equation (22). The parameters are chosen to be $\gamma = 2$ and (I) $\beta = 1280, \delta = 1$; (II) $\beta = 828.7, \delta = 1280$; (III) $\beta = 1, \delta = 1280$; (IV) $\beta = -828.7, \delta = 1280$; respectively.

5.2. TF approximation with box potential

In this section, we consider the box potential case, which confines the BEC in a bounded domain $\{|\mathbf{x}| \leqslant R\}$. Using a similar method for the harmonic potential case, we can obtain the analytical TF densities if the contact interaction and/or HOI dominates the ground state in equation (22). The analytical TF densities for different regimes which are shown in figure 3(b) are derived. The borderline of the three regimes is $\beta = O(\delta)$, which is different from the harmonic potential case.

Regime I: the β term is dominant, i.e. $\beta \gg 1$ and $\delta = o(\beta)$. The kinetic term and the HOI term are dropped and the time-independent MGPE in the radial variable r becomes

$$\mu\psi(r) = \beta\,|\psi|^2\psi, \quad 0 \leqslant r = |\mathbf{x}| < R, \tag{40}$$

with boundary condition $\psi(R) = 0$. Thus, the TF density is a constant, which can be uniquely determined by the normalization condition $\|\psi\| = 1$. Explicitly, the TF density is given by $n_{\mathrm{TF}}(r) = |\psi|^2 = \frac{\tilde{C}_d}{R^d}$, and $\mu_{\mathrm{TF}} = \frac{\tilde{C}_d\beta}{R^d}$, where $\tilde{C}_d$ is defined in the previous subsection.

It is obvious that the TF density is inconsistent with a zero boundary condition, thus a boundary layer appears in the ground-state density profile [24]. In fact, as shown in [24], for the case $d = 1$, an asymptotic analysis to match the boundary layers at $x = \pm R$ leads to the following matched density for $0 \leqslant r = |x| \leqslant R$ when $\beta \gg 1$ and $\delta \sim o(1)$,

$$n_{\mathrm{as}}(r) = |\psi_{\mathrm{as}}|^2 = \frac{1}{2R}(\tanh(\sqrt{\mu_{\mathrm{as}}}(R - r)))^2, \tag{41}$$

with the chemical potential $\mu_{\mathrm{as}} = \frac{1}{2R}\beta + \frac{1}{R}\sqrt{\frac{\beta}{2R}}$, and the energy $E_{\mathrm{as}} = \frac{1}{4R}\beta + \frac{2}{3R}\sqrt{\frac{\beta}{2R}}$. Similar matched densities can be derived for $d = 2, 3$.

From our numerical experience, the matched asymptotic density n_{as} provides much more accurate approximation to the ground state of equation (22), than the TF density n_{TF}, in the parameter regime $\beta \gg 1$ and $\delta = O(1)$.

Regime II: both β and δ are important, i.e. $\beta = O(\delta)$ as $\delta \to \infty$. We assume that $\beta = C_0\delta$, with $\delta \gg 1$ for some constant $C_0 > 0$.

Omitting the less important kinetic part, the radially symmetric time-independent MGPE reads

$$\mu\psi(r) = C_0\delta\,|\psi|^2\psi - \delta\nabla^2(|\psi|^2)\psi, \quad r < R, \tag{42}$$

with $\psi(R) = 0$. The above equation can be simplified for density $n(r) = |\psi|^2$ in d dimensions as

$$\frac{\mu}{\delta} = C_0 n(r) - \partial_{rr}n - \frac{d-1}{r}\partial_r n, \tag{43}$$

with $n(R) = 0$, and at $r = 0$ with $n'(0) = 0$. Equation (43) can be solved analytically.

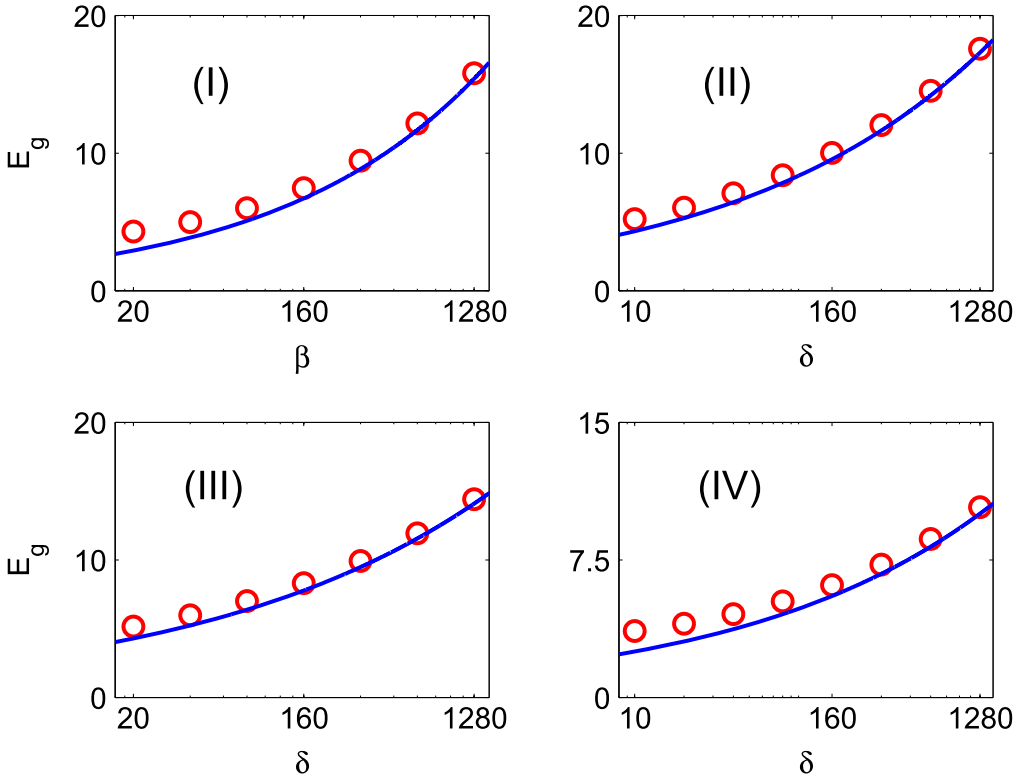

(a) comparison of energy (harmonic potential case)

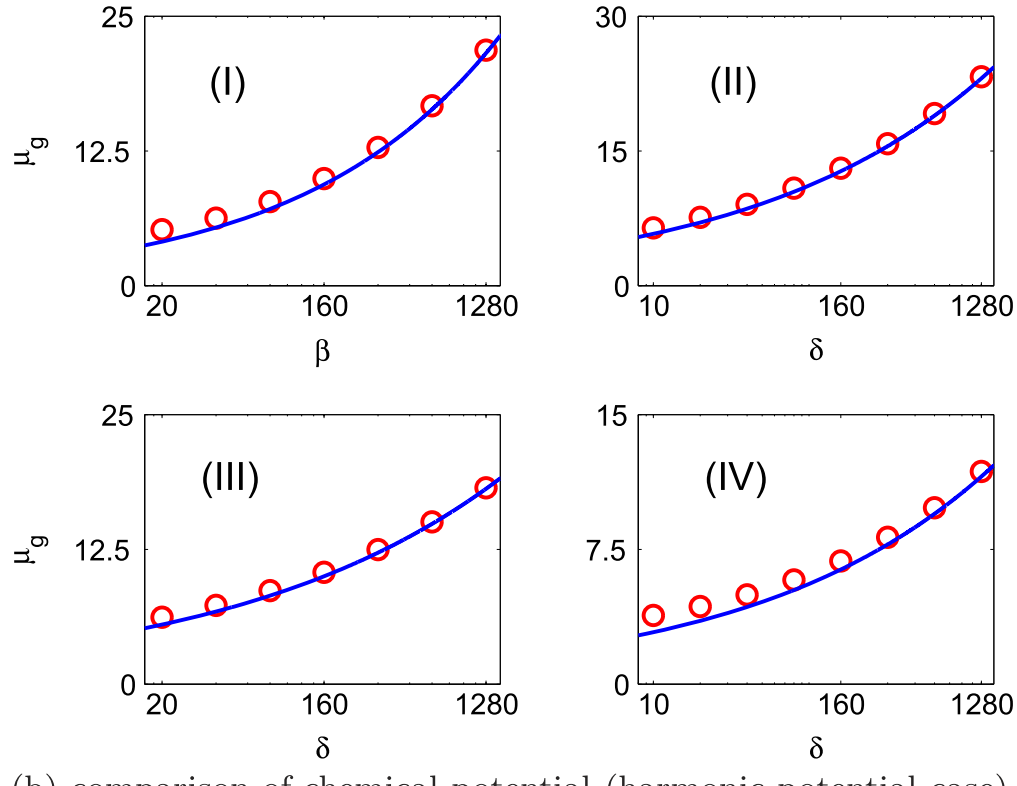

(b) comparison of chemical potential (harmonic potential case)

Figure 5. Comparisons of numerical energies and chemical potentials with TF approximations, the harmonic potential case. The 3D problem is considered here. Blue line: Thomas–Fermi approximation, and red circles: numerical results obtained from the equation (22). The parameters are chosen to be $\gamma = 2$ and (I) $\delta = 1$, (II) $\beta = 5\delta^{\frac{5}{7}}$, (III) $\beta = 1$, (IV) $\beta = -5\delta^{\frac{5}{7}}$, respectively.

The TF density, or the solution of the boundary value problem (43), is given explicitly as

$$n_{\rm TF}(r) = |\psi_{\rm TF}|^2 = \frac{\mu_{\rm TF}}{a^2\delta}\left[1 - \frac{f_{a,d}(r)}{f_{a,d}(R)}\right], \tag{44}$$

where $a = \sqrt{C_0}$, $f_{a,d}(r)$ is defined in equation (30) and $\mu_{\rm TF} = \tilde{C}_d a^2\delta \Big/ \left(R^d - d\frac{\int_0^R f_{a,d}(r)r^{d-1}dr}{f_{a,d}(R)}\right)$ with $\tilde{C}_d$ defined in equation (26). Further, we have $E_{\rm TF} = \mu_{\rm TF}/2$,

Regime III: δ term is dominant, i.e. $\delta \gg 1$, $\beta = o(\delta)$. The kinetic term and the β term are dropped. The corresponding stationary MGPE for the ground state reads

$$\mu\psi = -\delta\nabla^2(|\psi|^2)\psi, \tag{45}$$

with boundary condition $\psi(R) = 0$.

Solving the equation and using the normalization condition, we obtain the TF density as

$$n_{\rm TF}(r) = |\psi_{\rm TF}|^2 = \frac{(d+2)\tilde{C}_d(R^2 - r^2)_+}{2R^{d+2}}, \tag{46}$$

with chemical potential $\mu_{\rm TF} = \tilde{C}_d d(d+2)\delta/R^{d+2}$ and energy $E_{\rm TF} = \mu_{\rm TF}/2$.

Regime IV: i.e. $\beta = -C_0\delta$, with $\delta \gg 1$ for some constant $C_0 > 0$.

Intuitively, if C_0 is small, the repulsive HOI δ term is dominant and the particle density will still occupy the entire domain. If C_0 is sufficiently large, the attractive β interaction becomes the major effect, where the particles are self-trapped and the density profile concentrating in a small portion of the domain. Therefore, unlike the corresponding harmonic potential case, we have two different situations here.

By a similar procedure as for regime II, we get

$$\frac{\mu}{\delta} = -C_0 n(r) - \partial_{rr}n - \frac{d-1}{r}\partial_r n, \tag{47}$$

with $n(R') = 0$ and R' to be determined. In the first situation, the density spreads over the whole domain and thus $R' = R$; in the second situation, the density is constrained to a small region $[0, R']$, where $0 < R' < R$.

Case I: i.e. $C_0 \leqslant C_{\rm cr}$, where $C_{\rm cr} = \hat{R}^2/R^2$ and $\hat{R}$ is the first positive root of $g'_{a,d}(r/a) = 0$, where $g'_{a,d}(r)$ is defined in equation (36) with $a = \sqrt{C_0}$. As mentioned before, because of the relatively weak attractive interaction, we have the following boundary conditions at the boundary: $n(R) = 0$, $n'(0) = 0$.

The TF density, or solution of equation (47), can be expressed as:

$$n_{\rm TF} = |\psi_{\rm TF}|^2 = -\frac{\mu}{a^2\delta}\left[1 - \frac{g_{a,d}(r)}{g_{a,d}(R)}\right], \tag{48}$$

with $\mu_{\rm TF} = \tilde{C}_d a^2\delta \Big/ \left(d\frac{\int_0^R g_{a,d}(r)r^{d-1}dr}{g_{a,d}(R)} - R^d\right)$ and $E_{\rm TF} = \mu_{\rm TF}/2$, where $\tilde{C}_d$ is given in (26).

In fact, the condition $C_0 \leqslant C_{\rm cr}$, which is equivalent to $aR \leqslant \hat{R}$, is necessary. A simple argument for $d = 2, 3$ case is as follows. If $aR > \hat{R}$, we know from the property of $g_{a,d}(r)$ that the image of $g_{a,d}(r)$ for $r \in [0, \hat{R}]$ is exactly the image of $g_{a,d}(r)$ for all $r \geqslant 0$ and $g_{a,d}(R) \in (\min g_{a,d}(r), \max g_{a,d}(r))$. Then we can find $r_0 \in (0, \hat{R})$ such that $g_{a,d}(r_0) = g_{a,d}(R)$, and $1 - g_{a,d}(r)/g_{a,d}(R)$ changes signs for r around r_0. On the other hand, $1 - g_{a,d}(r)/g_{a,d}(R)$ cannot change signs in $[0, R]$ since the density must be non-negative. So we get a contradiction. Hence $aR \leqslant \hat{R}$, i.e. $C_0 \leqslant C_{\rm cr}$.

$g'_{a,d}$ at r/a can be computed as

$$g'_{a,d}(r/a) = \begin{cases} -a\sin(r), & d = 1, \\ -aJ_1(r), & d = 2, \\ a^2(r\cos(r) - \sin(r))/r^2, & d = 3, \end{cases} \tag{49}$$

and we have for 1D case, $\hat{R} = \pi$; for 2D case, $\hat{R} = 3.8317...$; for 3D case, $\hat{R} = 4.4934...$.

Case II: $C_0 > C_{\rm cr}$. As observed above, the densities drop to 0 before reaching the boundaries. Thus, free boundary conditions should be used as $n(\tilde{R}) = 0$, $n'(\tilde{R}) = 0$, $n'(0) = 0$, where $\tilde{R} < R$ is the boundary for the TF density that we want to find.

Hence the domain $[0, R]$ in case I needs to be replaced by $[0, \tilde{R}]$ with $n'(\tilde{R}) = 0$. Denoting $a = \sqrt{C_0}$ and using the solution in case I, we get $g'_{a,d}(\tilde{R}) = 0$, and $a\tilde{R} \leqslant \hat{R}$. Both conditions can only be satisfied when $a\tilde{R} = \hat{R}$. Hence $\tilde{R} = \hat{R}/a < R$.

Replacing R with $\hat{R}/a$ in the TF solution of case I, we obtain the analytical TF density

$$n_{\rm TF}(r) = |\psi_{\rm TF}|^2 = \frac{\tilde{C}_d a^d}{\hat{R}^d}\left[1 - \frac{g_{a,d}(r)}{g_{a,d}\left(\frac{\hat{R}}{a}\right)}\right], \tag{50}$$

where $\hat{R}$ is defined in case I. Further we have $\mu_{\rm TF} = -\tilde{C}_d a^{d+2}\delta/\hat{R}^d$ and $E_{\rm TF} = \mu_{\rm TF}/2$.

In figure 6, we compare the analytical TF densities listed above with the ground state obtained from numerical results via equation (22) computed by the BEFD method [31] in the various parameter regimes discussed above. Figure 6 shows our analytical TF densities are good approximations for the ground states. Figure 7 compares the chemical potentials and energies between the TF approximations and the numerical values by solving equation (22).

6. Conclusion

We have presented the mean-field modified Gross–Pitaevskii equations for quasi-1D, equation (14), and quasi-2D, equation (19), BECs with a higher-order interaction (HOI) term. These equations are based on a rigorous dimension reduction from the full 3D MGPE with the assumptions that the energy separations in radial and longitudinal directions scale differently in the strongly anisotropic aspect ratio limit, and the wave function can be separated into radial and longitudinal variables. By carefully studying the energy separation, we obtain the correct radial or longitudinal states used in the dimension reduction. In particular, it is quite interesting that the radial states have to be taken in a form

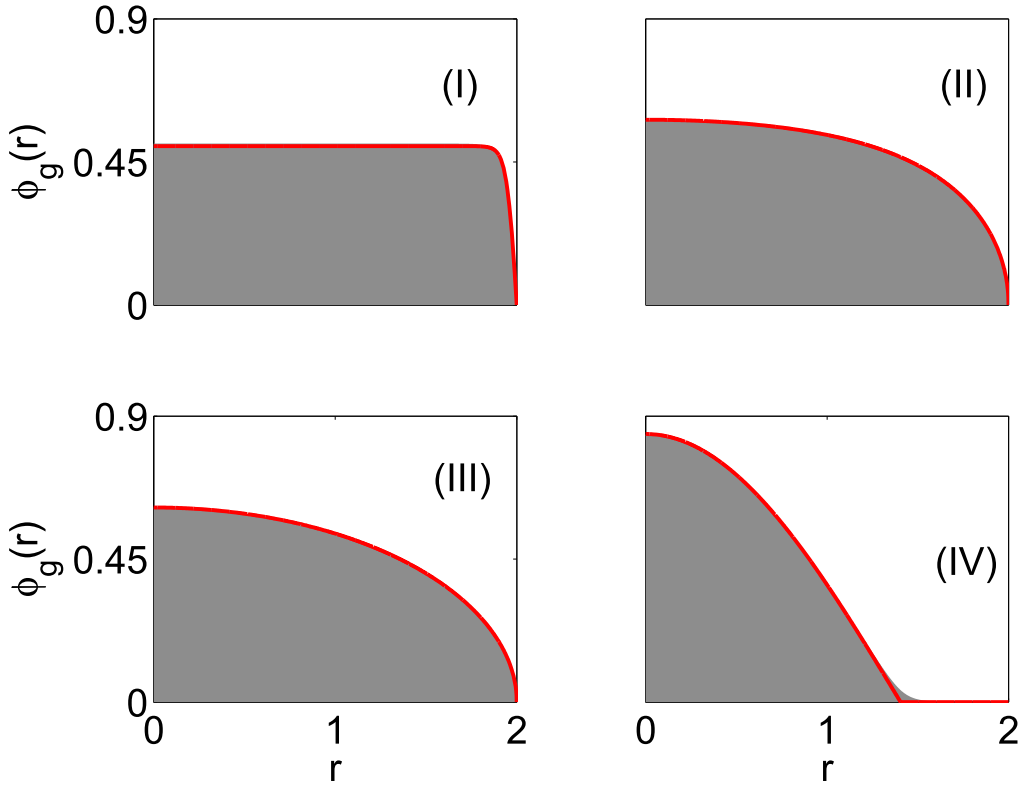

Figure 6. Comparisons of 1D numerical ground states with TF densities, the box potential case in region I, II, III and IV, which are defined in figure 3(b). Red line: analytical TF approximation, and shaded area: numerical solution obtained from (22). Domain is $\{r|0 \leqslant r < 2\}$ and the corresponding βs and δs are (I) $\beta = 1280$, $\delta = 1$; (II) $\beta = 320$, $\delta = 160$; (III) $\beta = 1$, $\delta = 160$; (IV) $\beta = -400$, $\delta = 80$.

different from the ground state of radial harmonic potential in the quasi-1D BEC, which is counterintuitive compared with the conventional GPE. Our result shows that quasi-1D and quasi-2D BECs with HOI are governed by a modified contact interaction term and a modified HOI term, and all the equations for quasi-1D and quasi-2D BECs have the same form as the 3D MGPE.

We have computed the ground states of our 1D and 2D equations numerically and compared them with the ground states of the 3D MGPE, and we find excellent agreements. We have also determined Thomas–Fermi approximation in various parameter regimes with both box potential and harmonic potential, for the 1D, 2D and 3D cases. TF approximations become very complicated in the presence of HOI since HOI competes with contact interaction.

Appendix A. Derivation of the quasi-1D equation

Under the assumption in section 3, we take the ansatz

$$\psi(x, y, z, t) = \mathrm{e}^{-\mathrm{i}\mu_{2D}t}\chi_{2D}(x, y)\psi_{1D}(z, t), \tag{A1}$$

where the transverse state is frozen, i.e. χ_{2D} is independent of time. We take χ_{2D} to be the radial minimum energy state because the energy separation is much larger in the radial direction than that in the longitudinal z-direction.

Substituting (A1) into equation (8), we can get the equations for ψ_{1D} for appropriate μ_{2D} as

$$\begin{aligned}\mathrm{i}\partial_t\psi_{1D}(z, t) \;=\; &\Big[-\frac{1}{2}\partial_{zz} + V_{1D}(z) + \beta_1|\psi_{1D}|^2 \\ &- \delta_1(\partial_{zz}|\psi_{1D}|^2)\Big]\psi_{1D},\end{aligned} \tag{A2}$$

where $V_{1D}(z) = \frac{1}{2}z^2$,

$$\beta_1 = \beta\iint|\chi_{2D}|^4\mathrm{d}x\mathrm{d}y + \delta\iint|\nabla_\perp|\chi_{2D}|^2|^2\mathrm{d}x\mathrm{d}y, \tag{A3a}$$

$$\delta_1 = \delta\iint|\chi_{2D}|^4\mathrm{d}x\mathrm{d}y, \tag{A3b}$$

and $\nabla_\perp = (\partial_x, \partial_y)^T$. It remains to determine χ_{2D} and we are going to use the criteria that the energy separation scales are different in different directions. In order to do this, we need to calculate the energy scale in the z-direction. Hence, we take the stationary states (ground states) of (A2) as

$$\psi_{1D}(z, t) = \mathrm{e}^{-\mathrm{i}\mu_{1D}t}\phi_{1D}(z). \tag{A4}$$

Combining equations (A1) and (A4), and following the way to find equation (A2), we can derive the equations for

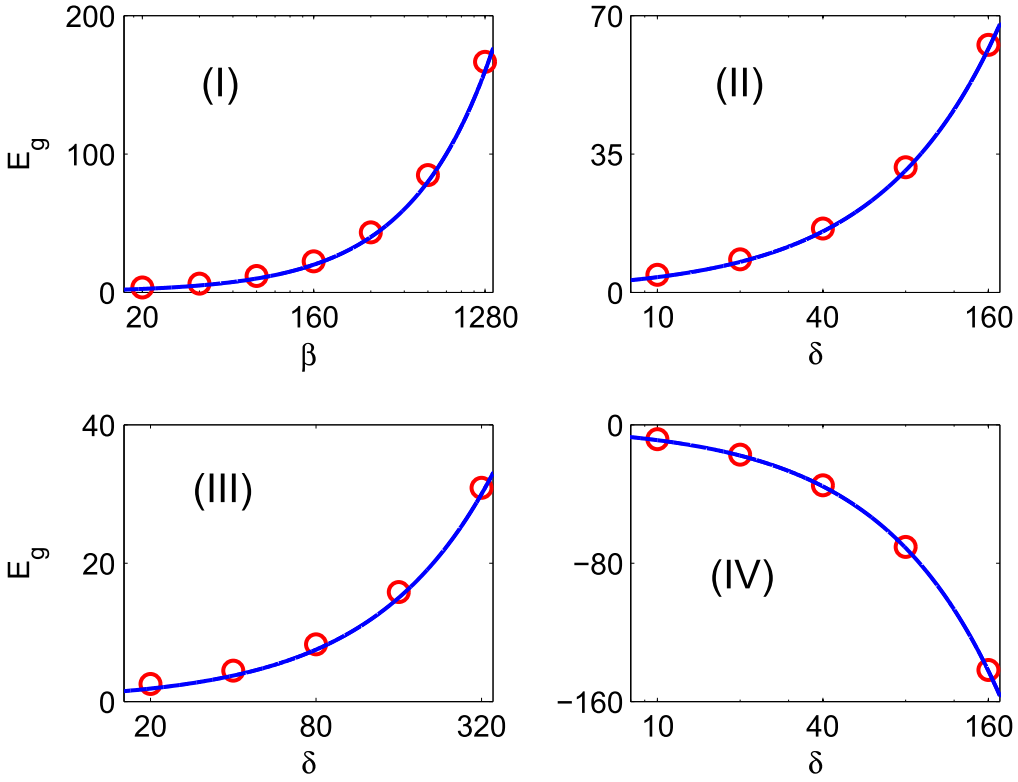

(a) comparison of energy (box potential case)

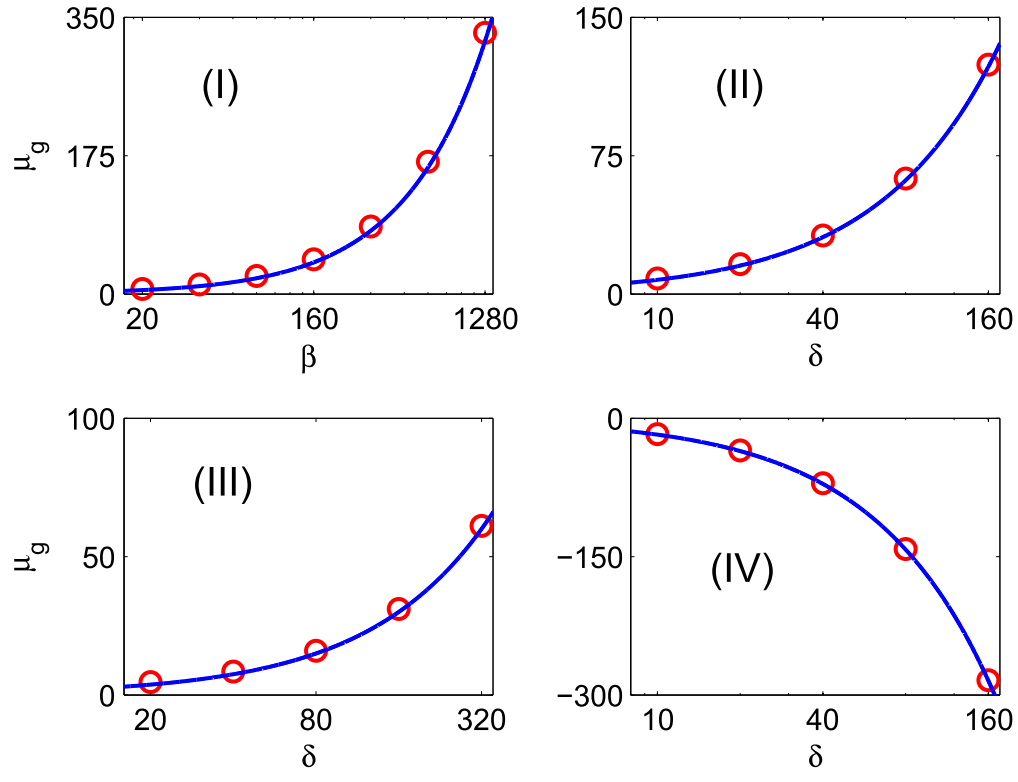

(b) comparison of chemical potential (box potential case)

Figure 7. Comparisons of numerical energies and chemical potentials with TF approximations, the box potential case. The 1D problem is considered here. Blue line: analytical TF approximation, and red circles: numerical results obtained from (22). The parameters are chosen to be (I) $\delta = 1$, (II) $\beta = 2\delta$, (III) $\beta = 1$, (IV) $\beta = -5\delta$, respectively, and domain is $\{r|0 \leqslant r < 2\}$.

$\chi_{2D}(x, y)$ as

$$\mu_{2D}\chi_{2D} = -\frac{1}{2}\nabla_\perp^2\chi_{2D} + V_{2D}(r)\chi_{2D} + \beta_2|\chi_{2D}|^2\chi_{2D} - \delta_2(\nabla_\perp^2|\chi_{2D}|^2)\chi_{2D}, \tag{A5}$$

where $\nabla_\perp^2 = \partial_{xx} + \partial_{yy}$, the radially symmetric potential $V_{2D} = \frac{\gamma^2}{2}(x^2 + y^2)$,

$$\beta_2 = \beta\int|\phi_{1D}|^4\mathrm{d}z + \delta\int|\partial_z|\phi_{1D}|^2|^2\mathrm{d}z, \tag{A6a}$$

$$\delta_2 = \delta\int|\phi_{1D}|^4\mathrm{d}z. \tag{A6b}$$

To determine the frozen state χ_{2D}, we need minimize the energy of equation (A5), while parameters β_2 and δ_2 depends on ϕ_{1D}. So, in fact, we need to solve a coupled system simultaneously for χ_{2D} and ϕ_{1D}. For this purpose, we will consider the problem in the quasi-1D limit as $\gamma \to \infty$. Intuitively, the transverse direction is almost compressed to a Dirac delta function as $\gamma \to \infty$, so that a proper scaling is needed to obtain the correct form of χ_{2D}.

We will determine χ_{2D} via a self-consistent iteration as follows: given some β_2 and δ_2, under proper scaling as $\gamma \to \infty$, (i) drop the less important part to get approximate χ_{2D}, (ii) put χ_{2D} into equation (A2) to determine the longitudinal ground state ϕ_{1D}, (iii) use ϕ_{1D} to compute β_2 and δ_2, and then (iv) check if it is consistent.

In the quasi-1D regime, $\gamma \to \infty$, similar to the conventional GPE case, due to the strong confinement in transverse direction, the ground-state solution ϕ_{1D} is very flat in the z-direction, as both nonlinear terms exhibit repulsive interactions. It is easy to get the scalings of $\int|\partial_z|\phi_{1D}|^2|^2\mathrm{d}z = O(L^{-3})$, $\int|\phi_{1D}|^4\mathrm{d}z = O(L^{-1})$, where L indicates the correct length scale of ϕ_{1D}. Therefore β_2 and δ_2 are, by definition, of the same order since $L \to \infty$ in the quasi-1D limit.

For mathematical convenience, we introduce $\varepsilon = 1/\sqrt{\gamma}$ such that $\varepsilon \to 0^+$. In the radial variable, introduce the new scale $\tilde{r} = r/\varepsilon^\alpha$ and $\tilde{w}(\tilde{r}) = \varepsilon^\alpha\chi_{2D}(r)$ such that $\tilde{r} \sim O(1)$ and $\|\tilde{w}\| = 1$, then (A5) becomes

$$\mu_{2D}\tilde{w} = -\frac{\nabla_\perp^2\tilde{w}}{2\varepsilon^{2\alpha}} + \frac{\tilde{r}^2\tilde{w}}{2\varepsilon^{4-2\alpha}} + \frac{\beta_2}{\varepsilon^{2\alpha}}\tilde{w}^3 - \frac{\delta_2}{\varepsilon^{4\alpha}}\nabla_\perp^2(|\tilde{w}|^2)\tilde{w}. \tag{A7}$$

Notice that the term $\beta_2/\varepsilon^{2\alpha}\tilde{w}^3$ can be always neglected compared to the last term since $\beta_2 \sim \delta_2$ and $\varepsilon^{-\alpha} \ll \varepsilon^{-3\alpha}$ as $\varepsilon \to 0^+$. On the other hand, β_2 and δ_2 are both repulsive interactions while only the potential term confines the condensate. Thus, the correct leading effects (HOI or kinetic term) should be balanced with the potential term. Now, we are only left with two possibilities:

Case I: $-\frac{1}{2\varepsilon^{2\alpha}}\tilde{\nabla}^2{}_\perp\tilde{w}$ is balanced with term $\frac{\tilde{r}^2}{2\varepsilon^{4-2\alpha}}\tilde{w}$, and $\frac{\delta_2}{\varepsilon^{4\alpha}}\tilde{\nabla}^2{}_\perp(|\tilde{w}|^2)\tilde{\psi}$ is smaller. In this case, $\varepsilon^{2\alpha} \sim \varepsilon^{4-2\alpha}$. So we get $\alpha = 1$. Besides, we also need $\varepsilon^{-2\alpha} \gg \frac{\delta_2}{\varepsilon^{4\alpha}}$, i.e. $\delta_2 \ll \varepsilon^2$.

Case II: $\frac{\delta_2}{\varepsilon^{4\alpha}}\tilde{\nabla}^2{}_\perp(|\tilde{w}|^2)\tilde{w}$ is balanced with term $\frac{\tilde{r}^2}{2\varepsilon^{4-2\alpha}}\tilde{w}$, and $-\frac{1}{2\varepsilon^{2\alpha}}\tilde{\nabla}^2{}_\perp\tilde{w}$ is much smaller. In this case, $\frac{\delta_2}{\varepsilon^{4\alpha}} \sim \frac{1}{\varepsilon^{4-2\alpha}}$ and $\varepsilon^{-2\alpha} \ll \frac{1}{\varepsilon^{4-2\alpha}}$, i.e. $\alpha < 1$ and $\delta_2 \sim \varepsilon^{6\alpha-4}$.

We will check if the scaling is consistent for each case. *Case I*: since $\alpha = 1$, we have χ_{2D} as the ground state of the radial harmonic oscillator,

$$\chi_{2D}(r) = \frac{1}{\sqrt{\pi\varepsilon^2}}\mathrm{e}^{-\frac{r^2}{2\varepsilon^2}}, \tag{A8}$$

and

$$\iint|\chi_{2D}|^4\mathrm{d}x\mathrm{d}y = \frac{1}{2\pi\varepsilon^2}, \quad \iint|\nabla_\perp(|\chi_{2D}|^2)|^2\mathrm{d}x\mathrm{d}y = \frac{1}{\pi\varepsilon^4}.$$

Recalling β_1 and δ_1 in equation (A3), the parameters are in TF regime I (cf section 3), so in the z-direction we can get the approximate solution from section 3 as:

$$\phi_{1D} \approx \sqrt{\frac{((z^*)^2 - z^2)_+}{2\beta_1}}, \quad z^* = \left(\frac{3\beta_1}{2}\right)^{\frac{1}{3}}, \tag{A9}$$

By definition of δ_2 (A6b), we obtain

$$\delta_2 = \delta\int|\phi_{1D}|^4\mathrm{d}z = \frac{3\delta}{5}\left(\frac{2}{3\beta_1}\right)^{\frac{1}{3}}, \tag{A10}$$

while

$$\beta_1 \sim \delta\iint|\nabla_\perp(|\chi_{2D}|^2)|^2\mathrm{d}x\mathrm{d}y = \frac{\delta}{\pi\varepsilon^4}. \tag{A11}$$

Combining (A10) and (A11), we get $\delta_2 = O(\varepsilon^{\frac{4}{3}})$. But this contradicts the requirement that $\delta_2 \ll \varepsilon^2$. Thus case I is inconsistent.

Case II: as the δ_2 term is more significant than the kinetic term, we solve $\mu_{2D} = r^2/2\varepsilon^4 - \delta_2\nabla_\perp^2|\chi_{2D}|^2$ within the support of $\chi_{2D}(r)$ and get

$$\chi_{2D}(r) = \frac{(R^2 - r^2)_+}{\sqrt{32\varepsilon^4\delta_2}}, R = 2a\varepsilon, a = \left(\frac{3\delta_2}{2\pi\varepsilon^2}\right)^{\frac{1}{6}}. \tag{A12}$$

Hence, we know

$$\iint|\chi_{2D}|^4\mathrm{d}x\mathrm{d}y = \frac{3}{10\delta_2}\left(\frac{3\delta_2}{2\pi\varepsilon^2}\right)^{\frac{2}{3}}, \tag{A13}$$

$$\iint|\nabla_\perp|\chi_{2D}|^2|^2\mathrm{d}x\mathrm{d}y = \frac{1}{2\delta_2\varepsilon^2}\left(\frac{3\delta_2}{2\pi\varepsilon^2}\right)^{\frac{1}{3}}. \tag{A14}$$

Again, recalling β_1 and δ_1 in equation (A3), the parameters are in TF regime I (cf section 3), so in the z-direction we can get the approximate solution from section 3 as equation (A9). Using $\phi_{1D}(z)$ in equation (A9), we can compute

$$\delta_2 = \delta\int|\phi_{1D}|^4\mathrm{d}z = \frac{3\delta}{5}\left(\frac{2}{3\beta_1}\right)^{\frac{1}{3}}, \tag{A15}$$

while

$$\beta_1 \sim \delta\int|\nabla_\perp|\chi_{2D}|^2|^2\mathrm{d}x\mathrm{d}y = \left(\frac{3}{2\pi}\right)^{\frac{1}{3}}\frac{\delta}{2\varepsilon^{\frac{8}{3}}\delta_2^{\frac{2}{3}}}. \tag{A16}$$

Combining (A15) and (A16), we find $\delta_2 = \frac{2\cdot 3^{\frac{5}{7}}\pi^{\frac{1}{7}}\delta^{\frac{6}{7}}\varepsilon^{\frac{8}{7}}}{5^{\frac{9}{7}}}$, $\beta_1 \sim \frac{5^{\frac{6}{7}}}{3^{\frac{1}{7}}\cdot 4\pi^{\frac{3}{7}}}\delta^{\frac{3}{7}}\gamma^{\frac{12}{7}}$. Noticing the requirement that $\delta_2 \sim \varepsilon^{6\alpha-4}$, we get $\alpha = 6/7$, and it satisfies the other constraint $\alpha < 1$. Thus, case II is self-consistent, and it is the case that we should choose to derive the mean-field equation for the quasi-1D BEC. β_1, δ_1 can be obtained as in equation (15).

To summarize, we identify that χ_{2D} should be taken as equation (A12) and the mean-field equation (14) for quasi-1D BEC is derived.

With this explicit form of the approximate solutions, we can further get the leading-order approximations of chemical potential and energy for the original 3D problem. It turns out that $\mu_g^{3D} \approx \frac{9}{8}\mu_{2D}$ and $E_g^{3D} \approx \frac{7}{8}\mu_{2D}$, where μ_{2D} is computed approximately as before.

Appendix B. Derivation of the quasi-2D equation

Under the assumption in section 4, we take the ansatz

$$\psi(x, y, z, t) = \mathrm{e}^{-\mathrm{i}\mu_{1D}t}\chi_{1D}(z)\psi_{2D}(x, y, t), \tag{B1}$$

where the longitudinal state is frozen, i.e. χ_{1D} is the minimum energy state and the energy separation is much larger in the longitudinal z-direction than the radial direction.

Plugging equation (B1) into equation (8), we can get the equations for ψ_{2D} with appropriate μ_{1D} as

$$\begin{aligned}\mathrm{i}\partial_t\psi_{2D}(x, y, t) \;=\; &\Big[-\frac{1}{2}\nabla_\perp^2 + V_{2D}(x, y)\\ &+ \beta_2\,|\psi_{2D}|^2 - \delta_2(\nabla_\perp^2\,|\psi_{2D}|^2)\Big]\psi_{2D},\end{aligned} \tag{B2}$$

where the radially symmetric potential $V_{2D}(r) = \frac{1}{2}r^2$ and

$$\beta_2 = \beta\int|\chi_{1D}|^4\mathrm{d}x\mathrm{d}y + \delta\int|\partial_z|\chi_{1D}|^2|^2\mathrm{d}z, \tag{B3a}$$

$$\delta_2 = \delta\int|\chi_{1D}|^4\mathrm{d}x\mathrm{d}y, \tag{B3b}$$

with $\nabla_\perp = (\partial_x, \partial_y)^T$ and $\nabla_\perp^2 = \partial_{xx} + \partial_{yy}$. It remains to determine χ_{1D} and we are going to use the same idea as that in the quasi-1D BEC. In order to do this, we need calculate the energy scale in the r-direction. Hence, we take the stationary states (ground states) of equation (B2) as

$$\psi_{2D}(r, t) = \mathrm{e}^{-\mathrm{i}\mu_{2D}t}\phi_{2D}(r). \tag{B4}$$

Combining equation (B1) with equation (B4), we can derive the equations for $\chi_{1D}(z)$ as

$$\begin{aligned}\mu_{1D}\chi_{1D} = &-\frac{1}{2}\partial_{zz}\chi_{1D} + V_{1D}(z)\chi_{1D}\\ &+ \beta_1\,|\chi_{1D}|^2\chi_{1D} - \delta_1(\partial_{zz}|\chi_{1D}|^2)\chi_{1D},\end{aligned} \tag{B5}$$

where $V_{1D}(z) = \frac{z^2}{2\gamma^2}$,

$$\beta_1 = \beta\int|\phi_{2D}|^4\mathrm{d}z + \delta\int|\nabla_\perp|\phi_{2D}\,|^2|^2\mathrm{d}z, \tag{B6a}$$

$$\delta_1 = \delta\int|\phi_{2D}|^4\mathrm{d}z. \tag{B6b}$$

We proceed similarly to the quasi-1D case. For mathematical convenience, denote $\varepsilon = \sqrt{\gamma}$ such that $\varepsilon \to 0^+$. Rescale z-variable as $\tilde{z} = z/\varepsilon^\alpha$, $\tilde{\chi}(\tilde{z}) = \varepsilon^{\frac{\alpha}{2}}\chi_{1D}(z)$ for some $\alpha > 0$. By removing the tildes, equation (B5) becomes

$$\begin{aligned}\mu_{1D}\chi = &-\frac{1}{2\varepsilon^{2\alpha}}\partial_{zz}\chi + \frac{z^2}{2\varepsilon^{4-2\alpha}}\chi + \frac{\beta_1}{\varepsilon^\alpha}\chi^3\\ &-\frac{\delta_1}{\varepsilon^{3\alpha}}(\partial_{zz}|\chi|^2)\chi.\end{aligned} \tag{B7}$$

Assuming that the scale is correct, then χ will be a regular function, independent of ε so that its norm will be $O(1)$. Now, we will determine the scale. Intuitively, for the same reason shown in the quasi-1D case, the term $\frac{\beta_1}{\varepsilon^\alpha}\chi^3$ can always be neglected compared to the HOI term. In addition, the potential term is the only effect that confines the condensate, and cannot be neglected. As a result, there are only two possibilities:

Case I: $-\frac{1}{2\varepsilon^{2\alpha}}\partial_{zz}\chi$ is balanced with term $\frac{z^2}{2\varepsilon^{4-2\alpha}}\chi$, and $\frac{\delta_1}{\varepsilon^{3\alpha}}(\partial_{zz}|\chi|^2)\chi$ is much smaller. In this case, $\varepsilon^{2\alpha} \sim \varepsilon^{4-2\alpha}$. So we get $\alpha = 1$. Besides, we also need $\varepsilon^{-2\alpha} \gg \frac{\delta_1}{\varepsilon^{3\alpha}}$, i.e. $\delta_1 \ll \varepsilon$.

Case II: $\frac{\delta_1}{\varepsilon^{3\alpha}}(\partial_{zz}|\chi|^2)\chi$ is balanced with term $\frac{z^2}{2\varepsilon^{4-2\alpha}}\chi$, and $-\frac{1}{2\varepsilon^{2\alpha}}\partial_{zz}\chi$ is much smaller. In this case, $\frac{\delta_1}{\varepsilon^{3\alpha}} \sim \frac{1}{\varepsilon^{4-2\alpha}}$ and $\varepsilon^{-2\alpha} \ll \frac{1}{\varepsilon^{4-2\alpha}}$, i.e. $\alpha < 1$ and $\delta_1 \sim \varepsilon^{5\alpha-4}$.

Now, we check the consistency of each case.

Case I. Since $\alpha = 1$, we can obtain $\chi_{1D}(z)$ as the ground state of the longitudinal harmonic oscillator as

$$\chi_{1D}(z) = \left(\frac{1}{\pi\varepsilon^2}\right)^{\frac{1}{4}}\mathrm{e}^{-\frac{z^2}{2\varepsilon^2}}, \tag{B8}$$

and the following quantities can be calculated:

$$\int|\chi_{1D}|^4\mathrm{d}z = \frac{1}{\sqrt{2\pi}\,\varepsilon}\;,\quad \int|(|\chi_{1D}|^2)'|^2\mathrm{d}z = \frac{1}{\sqrt{2\pi}\,\varepsilon^3}. \tag{B9}$$

By examining β_2 and δ_2 in equation (B2), we find β_2 is dominant as $\varepsilon \to 0^+$ and the ground state $\phi_{2D}(r)$ can be obtained as a TF approximation in parameter regime I, as shown in section 5,

$$\phi_{2D}(r) = \sqrt{\frac{(R^2 - r^2)_+}{2\beta_2}},\quad \text{where } R = \left(\frac{4\beta_2}{\pi}\right)^{\frac{1}{4}}. \tag{B10}$$

Then we can compute

$$\iint|\phi_{2D}|^4\mathrm{d}x\mathrm{d}y = \frac{2}{3\sqrt{\pi\beta_2}}, \tag{B11}$$

$$\iint|\nabla_\perp(|\phi_{2D}|^2)|^2\mathrm{d}x\mathrm{d}y = \frac{2}{\beta_2}. \tag{B12}$$

Having ϕ_{2D}, we can check the consistency of case I. By the definition of δ_1 in equation (B6), we get

$$\delta_1 = \delta\iint|\phi_{2D}|^4\mathrm{d}x\mathrm{d}y = \frac{2\delta}{3\sqrt{\pi\beta_2}}, \tag{B13}$$

while it follows from the definition of β_2 in equation (B3),

$$\beta_2 \sim \delta \int |(|\chi_{1D}|^2)'|^2 \mathrm{d}z = \frac{\delta}{\sqrt{2\pi}\,\varepsilon^3}. \tag{B14}$$

Combining equations (B13) and (B14), we obtain $\delta_1 = \frac{2}{3}\sqrt{\frac{\delta}{\pi}}(2\pi)^{\frac{1}{4}}\varepsilon^{\frac{3}{2}} = O(\varepsilon^{\frac{3}{2}}) = o(\varepsilon)$, which satisfies requirement for δ_1. Thus, case I is self-consistent.

Case II. In this case, we solve equation $\mu_{1D} = \frac{z^2}{2\varepsilon^4} - \delta_1 \partial_{zz}|\chi_{1D}|^2$ within the support of χ_{1D} and get

$$\chi_{1D}(z) = \frac{((z^*)^2 - z^2)_+}{2\varepsilon^2\sqrt{6\delta_1}}, \quad z^* = \left(\frac{45\delta_1\varepsilon^4}{2}\right)^{\frac{1}{5}}.$$

Then we have the identities as

$$\int |\chi_{1D}|^4 \mathrm{d}z = \frac{2}{63}\left(\frac{45}{2}\right)^{\frac{4}{5}}(\varepsilon^4\delta_1)^{-\frac{1}{5}}, \tag{B15}$$

$$\int |(|\chi_{1D}|^2)'|^2 \mathrm{d}z = \frac{2}{21}\left(\frac{45}{2}\right)^{\frac{2}{5}}(\varepsilon^4\delta_1)^{-\frac{3}{5}}. \tag{B16}$$

In the quasi-2D limit regime, i.e. $0 < \varepsilon \ll 1$, by the definitions of β_2 and δ_2 in equation (B3), we find that β_2 is dominant and ϕ_{2D} can be obtained as the TF density in parameter regime I shown in section 5, which is exactly the same as equation (B10).

Similar to the previous case, we can calculate

$$\delta_1 = \delta \iint |\phi_{2D}|^4 \mathrm{d}x\mathrm{d}y = \frac{2\delta}{3\sqrt{\pi\beta_2}}, \tag{B17}$$

where

$$\beta_2 \sim \delta \int |(|\chi_{1D}|^2)'|^2 \mathrm{d}z = \frac{2\delta}{21}\left(\frac{45}{2}\right)^{\frac{2}{5}}(\varepsilon^4\delta_1)^{-\frac{3}{5}}. \tag{B18}$$

Combining equations (B17) and (B18), we can get $\delta_1 \approx \frac{2}{45}\left(\frac{105\delta}{\pi}\right)^{\frac{5}{7}}\varepsilon^{\frac{12}{7}}$. But the requirement is $\delta_1 \sim \varepsilon^{5\alpha-4}$, so we get $\alpha = 8/7$. This contradicts the other requirement that $\alpha < 1$. In other words, case II is inconsistent.

In summary, only case I is consistent and χ_{1D} should be chosen as equation (B8). Thus, the mean-field equation for quasi-2D BEC is derived in equation (19) with the constants given in equation (20).

Appendix C. Rescaling with harmonic potential

In this section, we show how to distinguish the four extreme regions in the TF approximations of equation (22).

In d ($d = 3, 2, 1$) dimensions, introduce $\tilde{\mathbf{x}} = \frac{\mathbf{x}}{x_s}$, and $\tilde{\psi}(\tilde{\mathbf{x}}) = x_s^{d/2}\psi(\mathbf{x})$ such that x_s is the Thomas–Fermi radius of the wave function and then the Thomas–Fermi radius in the new scaling is $O(1)$. It is easy to check that such scaling conserves the normalization condition equation (10). Substituting $\tilde{\mathbf{x}}$ and $\tilde{\psi}$ into the time-independent version of (22) and then removing all ~, we get

$$\frac{\mu}{x_s^2}\psi = -\frac{1}{2x_s^4}\nabla^2\psi + \frac{\gamma_0^2|\mathbf{x}|^2}{2}\psi + \frac{\beta}{x_s^{2+d}}\psi^3 - \frac{\delta}{x_s^{4+d}}\nabla^2(|\psi|^2)\psi.$$

x_s is the length scale and the potential term is $O(1)$. To balance the confinement with repulsive interactions, we need $\frac{\beta}{x_s^{2+d}} \sim O(1)$ and/or $\frac{\delta}{x_s^{4+d}} \sim O(1)$. For simplicity, we require $\frac{\delta}{x_s^{4+d}} = 1$, then $x_s = \delta^{\frac{1}{4+d}}$, and further $\beta \sim O(x_s^{2+d}) \sim O(\delta^{\frac{2+d}{4+d}})$. So the borderline case is $\beta = C_0\delta^{\frac{2+d}{4+d}}$. If $C_0 \gg 1$, the β term is much more significant than the δ term; if $|C_0| \ll 1$, the δ term is much more significant than the β term.

References

[1] Anderson M H, Ensher J R, Matthewa M R, Wieman C E and Cornell E A 1995 *Science* **269** 198–201
[2] Davis K B, Mewes M O, Andrews M R, van Druten N J, Durfee D S, Kurn D M and Ketterle W 1995 *Phys. Rev. Lett.* **75** 3969–73
[3] Bradley C C, Sackett C A, Tollett J J and Hulet R G 1995 *Phys. Rev. Lett.* **75** 1687–90
[4] Dalfovo F, Giorgini S, Pitaevskii L P and Stringari S 1999 *Rev. Mod. Phys.* **71** 463
[5] Pethick C J and Smith H 2002 *Bose-Einstein Condensation in Dilute Gases* (Cambridge: Cambridge University Press)
[6] Pitaevskii L P and Stringari S 2003 *Bose-Einstein Condensation* (New York: Oxford University Press)
[7] Lieb E H, Seiringer R and Yngvason J 2000 *Phy. Rev.* A **61** 043602
[8] Hau L V, Busch B D, Liu C, Dutton Z, Burns M M and Golovchenko J A 1998 *Phys. Rev.* A **58** R54
[9] Bao W and Cai Y 2013 *Kinet. Relat. Mod.* **6** 1–35
[10] Holland M J, Jin D, Chiofalo M L and Cooper J 1997 *Phys. Rev. Lett.* **78** 3801
[11] Stamper-Kurn D M, Andrews M R, Chikkatur A P, Inouye S, Miesner H-J, Stenger J and Ketterle W 1998 *Phys. Rev. Lett.* **80** 2027
[12] Bao W, Jaksch D and Markowich P A 2003 *J. Comput. Phys.* **187** 318–42
[13] Esry B D and Greene C H 1999 *Phys. Rev.* A **60** 1451–62
[14] Andersen J O 2004 *Rev. Mod. Phys.* **76** 599–639
[15] Fu H, Wang Y and Gao B 2003 *Phys. Rev.* A **67** 053612
[16] Collin A, Massignan P and Pethick C J 2007 *Phys. Rev.* A **75** 013615
[17] Veksler H, Fishman S and Ketterle W 2014 *Phys. Rev.* A **90** 023620
[18] Garcia-Ripoll J J, Konotop V V, Malomed B A and Perez-Garcia V M 2003 *Math. Comput. Simul.* **62** 21–30
[19] Qi W, Liang Z and Zhang Z 2013 *J. Phys. B: At. Mol. Opt. Phys.* **46** 175301
[20] Qi X and Zhang X 2012 *Phys. Rev.* E **86** 017601
[21] Wamba E, Sabari S, Porsezian K, Mohamadou A and Kofané T C 2014 *Phys. Rev.* E **89** 052917
[22] Thøgersen M, Zinner N T and Jensen A S 2009 *Phys. Rev.* A **80** 043625
[23] Bao W, Ge Y, Jaksch D, Markowich P A and Weishaeupl R M 2007 *Comput. Phys. Commun.* **177** 832–50
[24] Bao W, Lim F Y and Zhang Y 2007 *Bull. Inst. Math.* **2** 495–532
[25] Salasnich L 2009 *J. Phys. A: Math. Theor.* **42** 335205

[26] Young-S L E, Salasnich L and Adhikari S K 2010 *Phys. Rev.* A **82** 053601
[27] Cai Y, Rosenkranz M, Lei Z and Bao W 2010 *Phys. Rev.* A **82** 043623
[28] Ben Abdallah N, Méhats F, Schmeiser C and Weishäupl R M 2005 *SIAM J. Math. Anal.* **47** 189–99
[29] Bao W, Le Treust L and Mehats F 2015 *Nonlinearity* **28** 755–72
[30] Görlitz A *et al* 2001 *Phys. Rev. Lett.* **87** 130402
[31] Bao W and Du Q 2004 *SIAM J. Sci. Comput.* **25** 1674–97
[32] Adhikari S and Malomed B A 2009 *Physica* D **238** 1402–12